Design and Operation of a Smart Graphene–Metal Hybrid Reflectarray at THz Frequencies

Arjun Singh*, Michael Andrello†‡, Erik Einarsson†§
Ngwe Thawdar‡, Josep Miquel Jornet*

*Department of Electrical and Computer Engineering
Northeastern University, Boston, MA, USA E-mail: {singh.arj,jmjornet}@northeastern.edu

†Department of Electrical Engineering
§Department of Materials Design and Innovation
University at Buffalo, Buffalo, NY, USA, E-mail: {maandrel,erikeina}@buffalo.edu

‡US Air Force Research Laboratory
Rome, NY, USA, E-mail: ngwe.thawdar@us.af.mil

***Abstract*—Terahertz (THz)-band (0.1 - 10 THz) communication is envisioned as a key wireless technology to fulfill the demand for dense networks and higher data rates. To overcome the complex THz communication channel, smart reflecting surfaces can be utilized to facilitate Non-Line of Sight (NLOS) communication and increase efficiency. In this light, the use of new 2D nanomaterials, such as graphene, to design reprogrammable reflectarrays is being explored. This paper presents a novel graphene–metal hybrid reflectarray for THz communications. The radiating element of the reflectarray is designed to have strong reflection efficiency and high tunability. The trade-offs in the design of the hybrid element are exhaustively studied. The ability to perform continuous dynamic beamforming is presented. Extensive numerical results are provided to demonstrate the functionality of the reflectarray to engineer NLOS paths for communication.**

***Index Terms*—Terahertz communications; Reflectarrays; Graphene plasmonics; Smart Reflecting Surfaces**

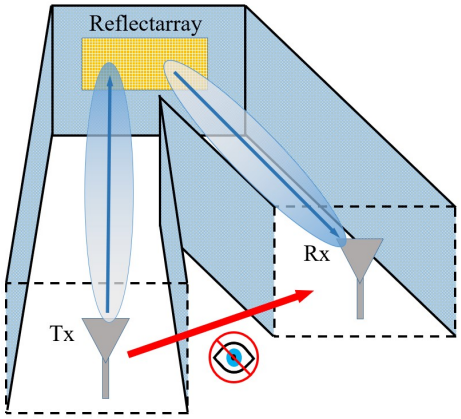

Fig. 1: Reflectarray for NLOS wireless communications.

I. Introduction

Terahertz (THz)-band communication is envisioned as a key wireless technology in fulfilling the demands and needs of future wireless communications [1], [2]. Already, the FCC has incentivized the spectrum above 95 GHz, with the aim of overcoming the spectrum scarcity problem and increase the capacity of wireless networks [3]. The THz band, between 0.1 - 10 THz, has multiple windows with up to tens and hundreds consecutive GHzs. Therefore, the development of a communications technology at THz frequencies eliminates the problem of bandwidth limitation to a large extent. Previously, the THz band remained unexploited due to several challenges. Among others, the lack of high power signal sources at the THz range, and the very high propagation losses at THz frequencies drastically limit the communication distance [4]. To overcome this limitation, beamforming antenna arrays have been proposed to improve effective power and increase the communication distance [5], as successfully demonstrated at lower frequencies [6]. These arrays improve radiation efficiency by concentrating the direction of the beam towards a Line of Sight (LOS) path or specular Non-Line of Sight (NLOS) paths between the transmitter and the receiver.

However, there are many scenarios in which beamforming at the communication ends is not sufficient or even possible. The presence of mobile or static obstacles can result in large signal losses, or worse, complete signal cut-off. Further, it is unlikely that low-cost low-complexity devices will be equipped with sophisticated beamforming architectures. It is then prudent to consider the engineering of several transmission paths within such a communication setup, and at the same time enable dense spatial multiplexing of users. The implementation of smart reflecting surfaces, in particular reflectarrays, is one such method to help facilitate the dense, dynamic and highly complex communications at the THz-band [7].

A reflectarray is a reflecting surface composed of radiating elements. The fundamental physics of reflectarrays are similar to antenna arrays. By controlling the response of each radiating element, different patterns are dynamically defined to intercept signals from specific directions and reflect them in a target

direction [8], [9]. Reflectarrays have been demonstrated to work efficiently at near THz frequencies [10]. However, current designs fall short of a dynamic beamforming response as the viable approaches applicable at lower frequencies become impractical. On the one hand, a variable capacitor can be connected to the element port to provide a “buffer" and delay the electrical current generated. We have utilized this approach in our previous work at 60 GHz [11]. To implement the same technique at THz frequencies however, variable capacitors with extremely small capacitance are required; an impractical design. Another method to produce phase delays at the radiating element is to utilize metallic stubs. For a dynamic phase control, nano and micro electro-mechanical systems (NEMS/MEMS) can be utilized to connect or disconnect these stubs to the element [12]. However, this approach discretizes the phase control and has an upper limit as the operating frequency reaches sub-THz [13].

The limitations of traditional methods in designing dynamic THz-band reflectarrays has motivated the exploration of alternative methods. One such method is the use of graphene in designing novel plasmonic devices. Graphene is a two-dimensional carbon material with excellent electrical properties, making it very well suited for propagating extremely high frequency signals [14]. In addition, it is shown that THz-frequency Surface Plasmon Polariton (SPP) waves can propagate on graphene. SPP waves are highly confined EM waves generated at the interface of a conductor and dielectric, with wavelengths as much as orders of magnitude smaller than their free-space EM counterparts. Further, the properties of these SPP waves can be dynamically tuned by changing the conductivity of graphene [5]. Utilizing graphene plasmonics, several reflectarrays are proposed for THz-band communications, as in [15]. However, a mismatch between the momentum of SPP waves on graphene and the free-space EM waves leads to weak reflection strength of graphene elements, and ultimately poorly performing reflecting strategies.

In this paper, we propose the design of a hybrid metal–graphene reflectarray. In our design, the reflectarray building block consists of a gold patch and a graphene-based stub, which are jointly designed and integrated. The metallic patch acts as a strong reflecting element, while the electrical tunability of the graphene-based stub is utilized to control the phase in a dynamic manner.

The remainder of this paper is organized as follows. In Sec. II, we present the design of the individual element and of the resulting reflectarray when intergatring the elements. In Sec. III, we explain the method of implementing phase control for dynamic beamforming. We analyse the performance of the reflectarray through full wave Finite Difference Frequency Domain (FDFD) numerical simulations, and present our results in Sec. IV. Finally, we conclude our paper in Sec. V.

II. Hybrid Reflectarray Design

In this section, we describe the design of the hybrid reflecting element and its assembly in large arrays. Our system is designed to operate at 1.5 THz (*true* THz frequencies),

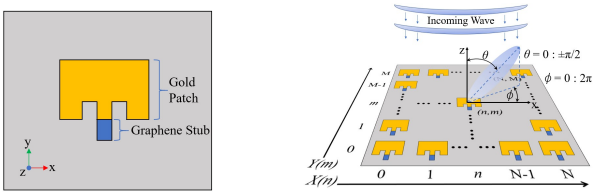

(a) Hybrid element (b) Reflectarray

Fig. 2: The design of the hybrid element and the resulting reflectarray

as this is the center frequency of our experimental setup for future system characterization. The same methodology can be utilized to design the system across the THz band.The resultant free-space wavelength λ_0 is then $199.8\,\mu\text{m}$.

A. Single Element Design and Principle

1) Patch: The metallic patch works as a broadside emitter on the basis of radiating slots. For optimal design efficiency at the desired frequency, the thickness of the substrate needs to be in the range of $0.003 - 0.05\ \lambda_0$, as given by [8].

The reflection coefficient, or the S11 parameter, is the accepted performance metric for a patch antenna. The lower the S11 in transmission, the higher the efficiency [8]. By the reciprocity principle, a good transmitting patch is also a good receiver. Since a reflectarray element is required to be a good receiver as well as a good transmitter, the patch so designed is a resonant reflectarray element [9].

The dimensions of the patch are modelled from the cavity model equations (1), (2) and (3), as per [8]:

$$W = \frac{c}{2f_0\sqrt{\frac{\varepsilon_r+1}{2}}}, \tag{1}$$

$$\varepsilon_{\text{eff}} = \frac{\varepsilon_r+1}{2} + \frac{\varepsilon_r-1}{2}[1+12h/W]^{-1/2}, \tag{2}$$

$$L = \frac{c}{2f_0\sqrt{\varepsilon_{\text{eff}}}} - 0.824h\left[\frac{(\varepsilon_{\text{eff}}+0.3)(\frac{W}{h}+0.264)}{(\varepsilon_{\text{eff}}-0.258)(\frac{W}{h}+0.8)}\right]. \tag{3}$$

Here, W and L are the width and the length of the patch antenna at a desired frequency of f_0 and h is the thickness of the substrate. ε_r represents the dielectric constant of the substrate, while ε_{eff} represents the effective dielectric constant, since the electric fields of the patch antenna undergo fringing at the boundary of the substrate.

2) Stub: We implement phase control through a graphene based stub, which acts as a waveguide with an active graphene layer [16]. The properties of the SPP waves generated in this waveguide are captured by the complex wave vector k_{spp}. More specifically, as shown in (4) and (5) the plasmonic wavelength λ_{spp} is dependent on the real part $\Re\{k_{\text{spp}}\}$, while

the propagation length L is dependent on the imaginary part $\Im\{k_{\rm spp}\}$.

$$\lambda_{\rm spp} = \frac{2\pi}{\Re\{k_{\rm spp}\}}, \tag{4}$$

$$L = \frac{1}{2\Im\{k_{\rm spp}\}}. \tag{5}$$

We find the complex wave vector as per the dispersion equation for SPP waves on graphene [17]:

$$-i\frac{\sigma^g}{\omega\varepsilon_0} = \frac{\varepsilon_1 + \varepsilon_2 \coth(k_{spp}d)}{k_{spp}}. \tag{6}$$

Here, σ^g is the conductivity of graphene, ε_1 is the relative permittivity of the dielectric above graphene (air), ε_2 is the relative permittivity of the dielectric below graphene (silicon dioxide), and d is the separation between graphene and the metallic ground plane. The conductivity model for graphene is obtained using the Kubo formalism [18] [19], given by the following equations:

$$\sigma^g = \sigma^g_{intra} + \sigma^g_{inter}, \tag{7}$$

$$\sigma^g_{intra} = i\frac{2e^2}{\pi\hbar^2}\frac{k_BT}{\omega + i\tau_g^{-1}}\ln\left[2\cosh\left(\frac{E_F}{2k_BT}\right)\right], \tag{8}$$

$$\sigma^g_{inter} = \frac{e^2}{4\hbar}\left[H(\frac{\omega}{2}) + i\frac{4\omega}{\pi}\int_0^\infty \frac{G(\epsilon) - G(\omega/2)}{\omega^2 - 4\epsilon^2}d\epsilon\right], \tag{9}$$

and

$$G(a) = \frac{\sinh(\hbar a/k_BT)}{\cosh(E_F/k_BT) + \cosh(\hbar a/k_BT)}. \tag{10}$$

where $\omega = 2\pi f$ is the angular frequency, $\hbar$ is the reduced Planck's constant, e is the electron charge, k_B is the Boltzmann constant, T is the temperature, E_F refers to the Fermi energy of the graphene sheet, and τ_g is the relaxation time of electrons in graphene. The intrinsic properties of graphene, among them the relaxation time, are set as per numerous experimental characterizations of graphene [20].

In such a setup, by changing the Fermi energy of the graphene layer (i.e., the highest energy level occupied by electrons in graphene), for example, by means of electrostatic bias, the SPP wave propagation speed is modified. A change in propagation speed leads to a change in phase of the SPP wave at the output of the stub. Due to the nonlinear nature of these equations, a numerical analysis is required to derive stub dimensions so as to establish a phase delay of 2π radians, with minimal power dissipation across the graphene layer.

3) Joint Design: The hybrid element is obtained by combining the metallic patch and the graphene stub. The metallic patch converts the resonant incident wave to an electrical current, generating SPP waves which propagate across the graphene stub. The SPP wave travels across the length of the graphene stub and back towards the patch, before being radiated back as an EM wave.

Following the transmission line theory of graphene [21], it is understood that changing the Fermi energy of graphene nano-ribbons causes a change in the characteristic impedance. Therefore a mismatch at the metal–graphene interface is expected. However, in the absence of active port elements, the mismatch cannot be studied and accounted for. Instead, a numerical analysis is performed to determine the jointly optimized design. Figure 2a shows a schematic of the final design; with the geometry optimized as per the principle outlined. The dimensions of the hybrid element are summarized in Table I.

TABLE I: Hybrid Element Dimensions

Substrate thickness	$2.3\,\mu$m
Substrate permittivity	$4\varepsilon_0$
Patch width	$63.2\,\mu$m
Patch length	$49.94\,\mu$m
Stub length	$15\,\mu$m
Stub width	$10\,\mu$m
Inlet width	$9\,\mu$m
Inlet length	$18\,\mu$m
Graphene relaxation time	1 ps

B. Reflectarray Design and Principle

The reflectarray is designed following conventional array theory. The centre to centre separation between the elements is kept at $\lambda_0/2$. This spacing minimizes mutual coupling effects without creating grating lobes [8]. Therefore, mutual coupling effects are negligible. The hybrid reflectarray is presented in Fig. 2b. It is seen that the reflectarray is excited by an external source. Each element of the array is designed to have a certain beamforming weight, assigned through the application of a codebook. The resultant beam from the complete superposition of all the weighted elements is steered to the desired direction (θ, ϕ).

For the planar array in Fig. 2b, to direct an incident wave with free-space wavenumer of k_0 towards a direction (θ, ϕ), the progressive phase delay between the elements separated by a distance d needs to be Φ_{RA}, where

$$\Phi_{RA} = k_0(R_i - d\sin\theta(x_i\cos\phi + y_i\sin\phi)). \tag{11}$$

The correction term k_0R_i is added to account for the incremental inherent phase delay from the incidence angle of the beam. When the incoming wave is broadside, the correction term is rendered void.

III. Reflectarray Control

A. Codebook Design

To implement the required phase delay of each element at position n, m of the array in Fig. 2b as per Eq. (11), a codebook is defined, composed of effective weights of $W_{n,m}$, corresponding to the n, m element. $W_{n,m}$ is of the form Ae^{iB}, where A represents the magnitude of signal strength, and B represents the relative phase. The reflectarray is intended for phase control. Thus, it is clear that for a complete continuous beamformed array, the weights required are of the form

$$W_{codebook} \in [1e^{i0}, 1e^{i2\pi}]. \tag{12}$$

The application of the derived codebook to the reflectarray results in the reflection of the incident wave in the particular

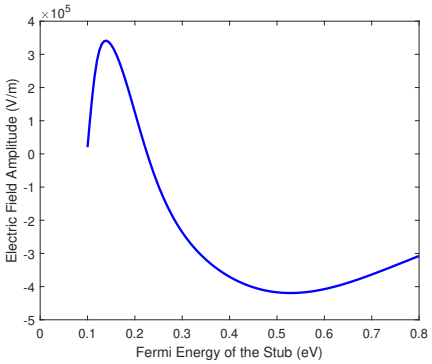

Fig. 3: Amplitude of the electric field at the output of the stub as the Fermi energy of the graphene-based stub is varied.

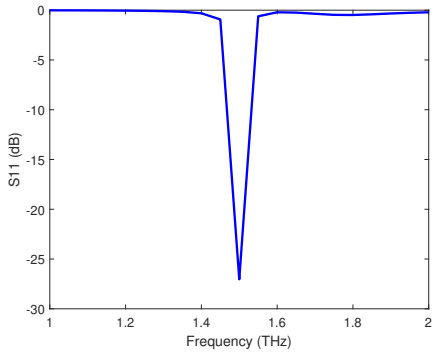

Fig. 4: Frequency response of the hybrid element. Resonance is observed at 1.5 THz.

desired direction. In the hybrid array, the codebook is applied by varying the Fermi energy of the graphene stub $EF_{stub_{n,m}}$. Thus, the effective complex weight $W_{n,m}$ is mapped to a particular stub Fermi energy of that element.

$$W_{n,m} \mapsto EF_{stub_{n,m}}. \tag{13}$$

B. Codebook Application

To implement the codebook, the relation between the Fermi energy of the stub and the relative phase delay is required. To develop this, the variation of the electric field amplitude at the output of the stub is found as a function of the Fermi energy of the stub, through full wave analysis of a single hybrid element, under transmission mode. This relation is presented in Fig. 3. It is seen that at different Fermi energy levels (all within the common range between 0.1 and 1 eV [18]), the corresponding output fields will exhibit a phase difference exceeding π radians. In reflection, the phase difference is doubled, and therefore complete phase control with 2π radians is possible.

IV. Results

In this section, we numerically investigate the performance of the single element and reflectarray, in terms of the the phase control and beamforming capabilites, respectively. Considering the computational cost of the numerical simulations, we restrict our analyses to a linear array. In the lack of mutual coupling effects as in our design, a planar array can be simplified to a combination of two linear arrays [8], and therefore the analyses presented are sufficient to characterize performance metrics.

A. Single Element Efficiency and Control

Figure 4 represents the relationship between the S11 parameter and the operating frequency of the hybrid element, through discrete port excitation at the input end of the graphene stub (transmission mode). At 1.5 THz, the S11 parameter is -27 dB, indicating resonance.

The derived relation between effective phase delay and Fermi energy of the stub is presented in Fig. 5. It is seen that within the common range of Fermi energies, complete phase control is possible.

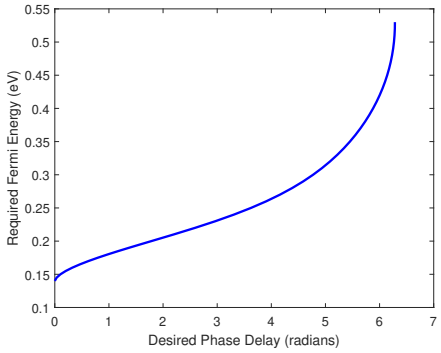

Fig. 5: The relation between the desired phase delay and the required Fermi energy of the graphene-based stub of the element.

The magnitude of reflection from the hybrid element is presented in Fig. 6, benchmarked to the signal strengths of metallic and graphene patches, all resonant at 1.5 THz. The metallic patch has the strongest signal reflection, albeit without beamforming support. The hybrid element has slight signal power attenuation due to power dissipation across the graphene stub while supporting total phase control for beamforming. In the case of the graphene only patch, a severely truncated reflecting signal is observed, due to the SPP-EM mismatch.

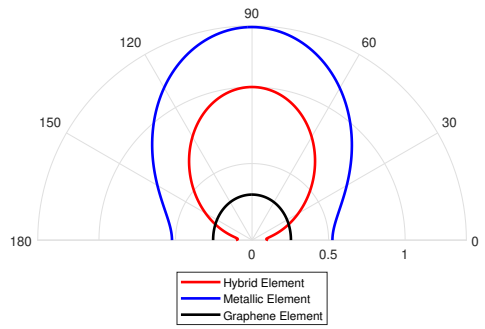

Fig. 6: A comparison between the normalized reflected power from the three different element designs.

B. Reflectarray Beamforming Analysis

To assess the dynamic beamforming capability of the reflectarray, a 4×1 reflectarray is analyzed. Figure 7 presents the resultant far-field radiation patterns of the reflected beam obtained from the implementation of the four different codebooks $C0$, $C1$, $C2$ and $C3$, designed to reflect a normal incident plane wave towards (θ, ϕ) = (0°,0°), (0°,15°), (0°,30°), and (0°,45°), respectively. Table. II presents the derived codebooks. It is seen that the hybrid reflectarray successfully reflects the beam in the intended directions.

TABLE II: The Derived Codebooks

Codebooks	Fermi Energy of Stubs			
	$EF_{stub_{0,0}}$	$EF_{stub_{1,0}}$	$EF_{stub_{2,0}}$	$EF_{stub_{3,0}}$
$C0$	0.5 eV	0.5 eV	0.5 eV	0.5 eV
$C1$	0.14 eV	0.176 eV	0.198 eV	0.212 eV
$C2$	0.14 eV	0.197 eV	0.232 eV	0.3 eV
$C3$	0.14 eV	0.208 eV	0.287 eV	0.159 eV

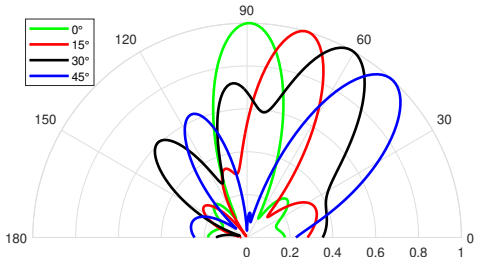

Fig. 7: The far-field radiation patterns of the reflected beam from the application of the codebooks in Table II to a 4×1 reflectarray.

V. Conclusion

In this paper, we have proposed a novel metal/graphene hybrid reflectarray. We successfully leverage the excellent reflection capabilities of micro-strip patches, and the excellent tunability of the graphene based stub to provide dynamic beamforming capability for engineering smart reflecting surfaces. Our future work is aimed at fabricating and experimentally testing the proposed structure.

Acknowledgements

(a) The State University of New York at Buffalo acknowledges the U.S. Government's support in the publication of this paper. This material is based upon work funded by AFRL, under AFRL Grant No. FA8750-19-1-0502. (b) Any opinions, findings, and conclusions or recommendations expressed in this material are those of the author(s) and do not necessarily reflect the views of AFRL. Approved for Public Release; Distribution Unlimited: 88ABW-2019-5678.

References

[1] R. Piesiewicz, T. Kleine-Ostmann, N. Krumbholz, D. Mittleman, M. Koch, J. Schoebei, and T. Kurner, "Short-range ultra-broadband terahertz communications: Concepts and perspectives," *IEEE Antennas and Propagation Magazine*, vol. 49, no. 6, pp. 24–39, 2007.

[2] T. S. Rappaport, Y. Xing, O. Kanhere, S. Ju, A. Madanayake, S. Mandal, A. Alkhateeb, and G. C. Trichopoulos, "Wireless communications and applications above 100 GHz: Opportunities and challenges for 6G and beyond," *IEEE Access*, vol. 7, pp. 78 729–78 757, 2019.

[3] US FCC, "Spectrum horizons: Petition for rulemaking to allow unlicensed operation in the 95-1,000 GHz band," 2019.

[4] I. F. Akyildiz, C. Han, and S. Nie, "Combating the distance problem in the millimeter wave and terahertz frequency bands," *IEEE Communications Magazine*, vol. 56, no. 6, pp. 102–108, 2018.

[5] I. F. Akyildiz and J. M. Jornet, "Realizing ultra-massive MIMO (1024×1024) communication in the (0.06–10) terahertz band," *Nano Communication Networks*, vol. 8, pp. 46–54, 2016, U.S. Patent No. 9,825,712, November 21, 2017 (Priority Date: Dec. 6, 2013).

[6] A. Simsek, S.-K. Kim, and M. J. Rodwell, "A 140 GHz MIMO transceiver in 45 nm SOI CMOS," in *2018 IEEE BiCMOS and Compound Semiconductor Integrated Circuits and Technology Symposium (BCICTS)*. IEEE, 2018, pp. 231–234.

[7] S. Nie, J. M. Jornet, and I. F. Akyildiz, "Intelligent environments based on ultra-massive MIMO platforms for wireless communication in millimeter wave and terahertz bands," in *ICASSP 2019-2019 IEEE International Conference on Acoustics, Speech and Signal Processing (ICASSP)*. IEEE, 2019, pp. 7849–7853.

[8] C. A. Balanis, *Antenna theory: analysis and design*. John Wiley & Sons, 2016.

[9] N. Payam, Y. Fan, and A. Z. Elsherbeni, *Reflectaray Antennas: Theory, Designs, and Applications*. Wiley-IEEE Press, 2018.

[10] T. Niu, W. Withayachumnankul, B. S.-Y. Ung, H. Menekse, M. Bhaskaran, S. Sriram, and C. Fumeaux, "Experimental demonstration of reflectarray antennas at terahertz frequencies," *Optics Express*, vol. 21, no. 3, pp. 2875–2889, 2013.

[11] X. Tan, Z. Sun, D. Koutsonikolas, and J. M. Jornet, "Enabling indoor mobile millimeter-wave networks based on smart reflect-arrays," in *IEEE INFOCOM 2018 - IEEE Conference on Computer Communications*, April 2018, pp. 270–278.

[12] B. Wu, A. Sutinjo, M. E. Potter, and M. Okoniewski, "On the selection of the number of bits to control a dynamic digital MEMS reflectarray," *IEEE Antennas and Wireless Propagation Letters*, vol. 7, pp. 183–186, 2008.

[13] S. V. Hum and J. Perruisseau-Carrier, "Reconfigurable reflectarrays and array lenses for dynamic antenna beam control: A review," *IEEE Transactions on Antennas and Propagation*, vol. 62, no. 1, pp. 183–198, 2013.

[14] A. K. Geim and K. S. Novoselov, "The rise of graphene," in *Nanoscience and Technology: A Collection of Reviews from Nature Journals*. World Scientific, 2010, pp. 11–19.

[15] E. Carrasco, M. Tamagnone, and J. Perruisseau-Carrier, "Tunable graphene reflective cells for THz reflectarrays and generalized law of reflection," *Applied Physics Letters*, vol. 102, no. 10, p. 104103, 2013.

[16] P. K. Singh, G. Aizin, N. Thawdar, M. Medley, and J. M. Jornet, "Graphene-based plasmonic phase modulator for terahertz-band communication," in *Proc. of the 10th European Conference on Antennas and Propagation (EuCAP)*. IEEE, 2016, pp. 1–5.

[17] V. Ryzhii, "Terahertz plasma waves in gated graphene heterostructures," *Japanese Journal of Applied Physics*, vol. 45, 2008.

[18] G. W. Hanson, "Dyadic green's functions and guided surface waves for a surface conductivity model of graphene," *Journal of Applied Physics*, vol. 103, no. 6, p. 064302, 2008.

[19] L. Falkovsky and A. Varlamov, "Space-time dispersion of graphene conductivity," *The European Physical Journal B*, vol. 56, no. 4, pp. 281–284, 2007.

[20] A. S. Mayorov, R. V. Gorbachev, S. V. Morozov, L. Britnell, R. Jalil, L. A. Ponomarenko, P. Blake, K. S. Novoselov, K. Watanabe, T. Taniguchi *et al.*, "Micrometer-scale ballistic transport in encapsulated graphene at room temperature," *Nano letters*, vol. 11, no. 6, pp. 2396–2399, 2011.

[21] J. M. Jornet and I. F. Akyildiz, "Graphene-based nano-antennas for electromagnetic nanocommunications in the terahertz band," in *Proceedings of the Fourth European Conference on Antennas and Propagation*. IEEE, 2010, pp. 1–5.